RESEARCH ARTICLE

Methane Interface Desorption Mechanism in Geological Reservoirs After Natural Gas Hydrate Decomposition

Longhao Tang[1], **Tingyi Wang**[1,*], **Yunlei Liu**[1] **and Haigang Zhou**[1]

[1] Shengli Oilfield Technology Inspection Center, Sinopec, Dongying 257000, China

Abstract

The morphological transformation of methane hydrates during re-exploitation, caused by depressurization and changes in reservoir environment, significantly impacts hydrate extraction. The present study explores the adsorption and desorption behaviour of methane under different environmental factors by constructing a rock adsorption and desorption device, which can contribute to the efficient extraction of methane during the decomposition of methane hydrates. The findings demonstrate that reservoir temperature strongly promotes methane desorption. Desorption capacity increased markedly above $100°C$**, reaching** $9.4\ \mu g/g$ **at** $120°C$**, consistent with reduced adsorption enthalpy (**ΔH_{ads} **from** -4.2 **to** -5.2×10^{-3} **kJ/mol) and increased Gibbs free energy favoring desorption. In contrast, higher reservoir pressure enhanced the drag force of the driving fluid, with methane desorption showing a sharp increase at pressures around** 25 **MPa, although low pressures yielded only marginal improvements. In addition, methane desorption rose from** $5.3\ \mu g/g$ **in low-**CO_2 **formulations to** $8.2\ \mu g/g$ **at** 90% CO_2 **content, driven by increased drag force (from** 2.5×10^{-3} **N to** 4.3×10^{-3} **N) and reduced adsorption energy (from** 6.2×10^{-4} **N to** 4.8×10^{-4} **N). Among reservoir minerals, montmorillonite showed the highest methane desorption capacity due to its lowest adsorption enthalpy and strong electrostatic repulsion, followed by illite, while kaolinite exhibited the weakest desorption performance. In conclusion, the present study provides fundamental data for the desorption and efficient extraction of methane leaked into geological reservoirs after the decomposition of methane hydrates.**

Keywords: hydrate decomposition, reservoir energy, reservoir transformation, methane desorption, energy resource exploitation.

1 Introduction

The ongoing availability of fossil fuels is widely recognised as a primary catalyst for the rapid economic development witnessed across the globe, thereby significantly contributing to the advancement of human civilisation. This phenomenon has a tangible impact on various aspects of human life, including but not limited to quality of life and technological innovation. The ongoing extraction of fossil fuels invariably results in a diminution of geological reserves, thereby posing a grave challenge

Submitted: 28 December 2025
Accepted: 26 April 2026
Published: 06 May 2026

Vol. 2, **No.** 3, 2026.
10.62762/RS.2025.633924

***Corresponding author:**
✉ Tingyi Wang
wangtingyi180.slyt@sinopec.com

Citation
Tang, L., Wang, T., Liu, Y., & Zhou, H. (2026). Methane Interface Desorption Mechanism in Geological Reservoirs After Natural Gas Hydrate Decomposition. *Reservoir Science*, 2(3), 172–188.

to the stability of energy supply and industrial development [1, 2]. Concurrently, the substantial quantities of carbon dioxide (CO_2) and solid waste produced during the combustion of fossil fuels constitute a grave threat to the global environment and the greenhouse effect, thereby introducing irreversible and substantial challenges to the Earth's ecosystem upon which humanity is dependent [3]. In order to address and mitigate the continuous depletion of fossil fuel reserves and the resulting environmental pollution, it is imperative that energy scientists and petroleum engineers explore new energy forms [4]. A plethora of novel energy sources, including hydrogen, wind, and solar energy, have been shown to exhibit remarkable environmental friendliness, which is undoubtedly a significant advantage in the replacement of fossil fuels [5]. These devices have been demonstrated to have no effect on the levels of CO_2 gas in the atmosphere, thus avoiding the increasingly severe greenhouse effect and global temperature rise, and their application does not trigger subsequent environmental pollution [6, 7]. Nevertheless, the numerous drawbacks of new energy sources, such as weak stability and low energy storage efficiency, are also significant reasons why these energy sources cannot be widely promoted [8]. The majority of novel energy sources are contingent on external environmental factors, including wind and solar power [9]. It is evident that climate change and variations in weather patterns have the potential to impact the collection and conversion efficiency of wind and solar energy [10]. Additionally, the substantial quantities of electricity generated during periods of abundant sunshine, water, and high wind speeds cannot be expeditiously utilised for residential or industrial purposes, and the surplus electricity cannot be completely stored to address energy shortages during cloudy or windless periods [11, 12]. Consequently, while the exploration of novel energy sources is undoubtedly a commendable endeavour that addresses pressing environmental concerns, such as pollution and the greenhouse effect, the assurance of a continuous and stable energy supply remains of paramount importance [13, 14]. Despite the implementation of strategies such as tertiary oil recovery, fossil fuels, which are non-renewable energy sources in conventional reservoirs, are approaching extinction. A significant number of petroleum engineers are currently investigating unconventional reservoirs as a prospective alternative energy source. The potential of shale energy and hydrates in unconventional reservoirs has garnered the attention of petroleum engineers, who are exploring these resources as a promising avenue for energy production [15, 16].

Methane hydrates, a unique energy source, are notoriously challenging to extract from high-pressure reservoirs located at the ocean floor. Current extraction technologies are unable to process these hydrates due to the harsh conditions of their reservoir environment [17, 18]. Changes in the reservoir environment directly trigger adjustments in hydrate morphology, thereby allowing large numbers of methane molecules to escape their confinement and disperse within reservoir fractures [19, 20]. This transformation of methane hydrate morphology has two consequences. Firstly, it alters the efficiency of utilisation of methane during combustion. Secondly, it renders reservoir stabilisation measures and the handling of spilled methane gas crucial factors hindering the large-scale modification of methane hydrate reservoirs [21]. While there are relatively well-developed research schemes for methane reservoir extraction and adsorption behaviour, there is a paucity of detailed research on methane hydrate reservoir desorption. Li et al. [22] conducted a study on the mechanical properties of hydrate saturation (MHSS) and hydrate saturation (MHCS) under depressurization decomposition conditions. This study determined the effects of hydrate saturation, depressurization time, and stress level on their mechanical properties and depressurization gas production rate. The authors also determined that the lack of significant impact of the number of depressurization cycles on the gas production rate is due to the constant pore pressure. Wang et al. [23] conducted experiments using high-pressure mercury injection (MIP), low-pressure gas phase adsorption (L-TA), low-pressure gas phase adsorption (L-PA), and high-pressure methane isothermal adsorption to explore the control effect of pore structure development characteristics on the adsorbed gas content in deep coal reservoirs. However, the adsorption and desorption behaviour of methane hydrate following decomposition was not analysed and characterised in detail, thus resulting in a paucity of information regarding the efficiency of methane gas extraction during reservoir stimulation. The desorption behavior of methane reservoirs after the decomposition of methane hydrates directly affects the methane recovery efficiency, which will inevitably become another important branch for filling the energy shortage [24].

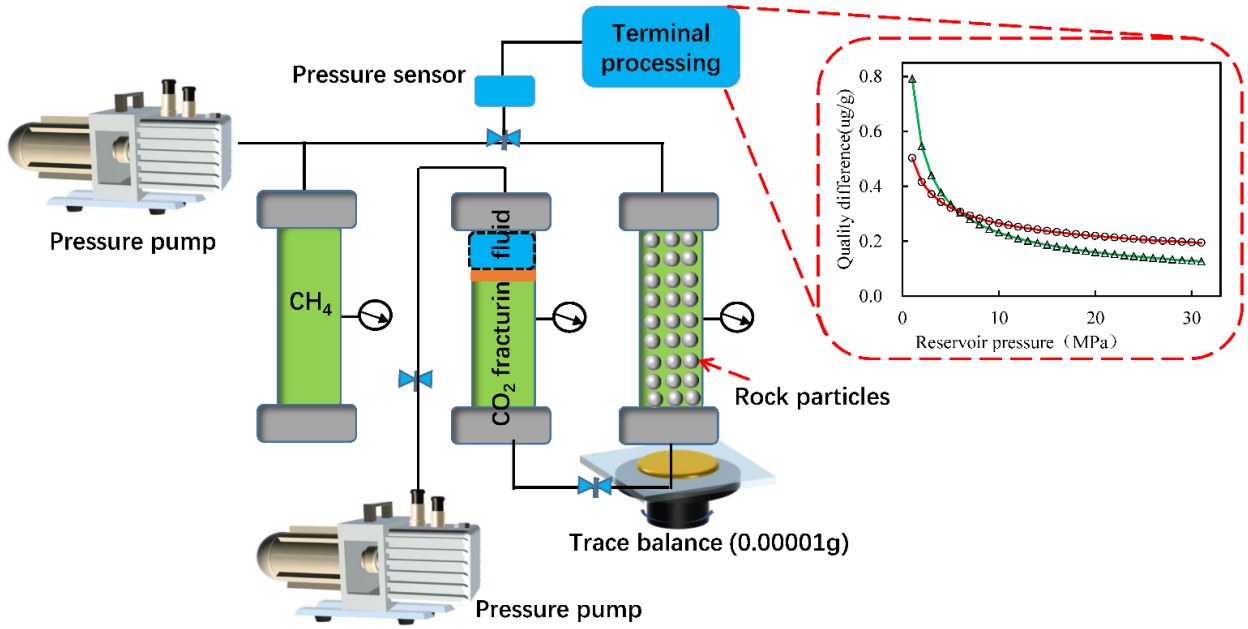

Figure 1. Evaluation device for gas adsorption/desorption behavior of methane hydrate decomposition in geological reservoirs.

The present study was conducted with the objective of investigating the methane desorption behaviour subsequent to the decomposition of methane hydrates. To this end, a multi-coupled evaluation device was constructed, which is capable of assessing methane adsorption and desorption behaviour on reservoir surfaces under a variety of conditions. Furthermore, the present study investigated the influence of various factors on methane desorption behaviour, based on the fundamental geological characteristics of methane hydrate reservoirs. The methane desorption mechanism was explained using a molecular dynamics model. Methane desorption from methane hydrate reservoirs has been identified as a promising solution to address the shortage of traditional energy sources, a development that is of critical importance in alleviating the prevailing energy crisis.

2 Materials and methods

2.1 Materials and Samples

Polyacrylamide was procured from Xilong Chemical Co., Ltd., and is principally utilised as a drag reducer. The polyacrylamide exhibits a degree of hydrolysis of 23% and a molecular weight of 8000. The cationic amine salts, which are small molecules, were procured from Aladdin Reagent (Shanghai) Co., Ltd., and their primary function is to inhibit clay swelling in shale. The primary function of fluorinated surfactants is to enhance reservoir flowback in methane-driven fluids, a process which concomitantly increases CO_2 viscosity in CO_2-driven fluids. Dimethylsiloxane finds primary application in the enhancement of viscosity and the stabilisation of speciation in fluids employed for CO_2-driven oil displacement. The reservoir core was taken from the Gulong Shale Oilfield block of Daqing Oilfield. It has a depth of 3125m and a porosity of 8.6% and a permeability of 3.5mD.

2.2 Experimental evaluation device

The reservoir rock samples were shale samples collected from a depth of 2500m in the reservoir. The samples were composed of finely pulverised granules, produced by subjecting the original materials to a crushing process, and subsequently filtered through a sieve with a mesh size of 100. The granules were meticulously packed into the designated sample container (Figure 1) and subsequently compacted. This facilitated the entry of CO_2 fracturing fluid into the sample container containing the rock particles for evaluation of adsorption/desorption behavior. The sample container, which was filled with rock particles, was subjected to an injection of CO_2 at a constant temperature of 30°C and a pressure of 37 MPa for a period of 1.5 hours. The purpose of this procedure was to ascertain the sealing performance of the evaluation device. Following the calibration of the reference container, the sample container was evacuated at 30°C for a 24-hour period (vacuum state), after which the adsorption/desorption behaviour of methane in the rock was evaluated. The adsorption behaviour experiment involved the extension of methane (in

the reference container) at a certain pressure into the sample container under the impetus of CO_2 fracturing fluid. The quantity of methane adsorbed was calculated using Boyle's law. Subsequent to the completion of the adsorption process, the valve between the reference container and the sample container was closed, thereby releasing a small amount of methane from the reference container and reducing the container pressure to 9 MPa (9 MPa selected to represent the typical reservoir pressure following hydrate dissociation in subsea sediments). Following a stabilisation period of two hours, the pressure within the container was measured in order to evaluate the amount of methane desorbed.

The calculation of desorption capacity is mainly based on the difference between the total mass after adsorption and the total mass after desorption, which can more intuitively reflect the absolute desorption capacity of methane on the surface of rock particles.

The adsorption equation V_{ads} and desorption equation Q_{des} of methane after the decomposition of reservoir hydrates on the reservoir rock are shown in Equations 1 and 2.

$$V_{ads} = \frac{1}{mRT}\left(P_1 V_{ref} Z(P_1, T) - [P_2(V_{ref} + V_{vid})Z(P_2, T)]\right) \quad (1)$$

where m is the mass of rock particles in the sample container, V_{ref} and V_{vid} are the known volume of the reference container and void volume in sample container. P_1 and P_2 are the pressure of the reference container before adsorption begins and the total pressure after adsorption equilibrium is reached, respectively. Z is the compression factor.

$$Q_{des} = \frac{M_{\text{post-ads}} - M_{\text{post-des}}}{m} \quad (2)$$

where $M_{\text{post-ads}}$ is the total mass of the system (rock + adsorbed gas) after adsorption equilibrium is reached. $M_{\text{post-des}}$ is the remaining total mass of the system after decompression and stabilization for two hours.

2.3 Molecular dynamics model of methane adsorption/desorption on rock surfaces

A molecular dynamics model incorporating methane and rock was constructed using molecular dynamics software. The model is principally employed to simulate and elucidate the adsorption and desorption behaviour and mechanisms of methane on rock surfaces. The initial step in the research process involved the manual creation of methane molecules and the subsequent optimisation of their molecular structure using the Forcite module. Concurrently, we fabricated shale crystal bags utilising the Supercell module and optimised their structure employing the COMPASS force field within the Forcite module. The shale model was based on the kerogen nanopore model, with a solid density of 1.220 g/cm3. The NVT and NPT systems of the kerogen nanopore model were periodically configured to simulate real reservoir environments. Finally, methane molecules were added to the kerogen nanopore model for mixing using the Sorption module, and the adsorption/desorption behaviour of methane on the kerogen nanopore model under different conditions was explored using the COMPASS force field.

2.4 Microscopic assessment of adsorption/desorption behavior on reservoir rock surfaces

In addition to quantifying the difference between methane adsorption and desorption masses on reservoir rock surfaces, specialised instrumentation enables direct observation of microscale adsorption features on the rock matrix. Microscopic imaging techniques, such as scanning electron microscopy (SEM) and transmission electron microscopy (TEM), can be employed to characterise methane adsorption–desorption behaviour of reservoir rocks under varying conditions, thereby providing critical insights into methane extraction efficiency following gas hydrate dissociation in geological reservoirs. Furthermore, Fourier-transform infrared spectroscopy (FT-IR) [25], combined with real-time quantitative analysis of methane adsorption–desorption dynamics under different reservoir conditions, was utilised to systematically evaluate and quantify the stimulation efficiency of natural gas hydrate reservoirs.

3 Results and discussion

3.1 Physical model of rock adsorption/desorption of methane after hydrolysis of methane hydrate

Figure 2 presents the adsorption and desorption characteristics of methane molecules on the geological reservoir surface following hydrate dissociation. As shown in Figure 2(a), the experimental adsorption data exhibit good agreement with the Langmuir isotherm model, which is consistent with the adsorption behaviour of many chemical species in geological reservoirs. A clear positive correlation

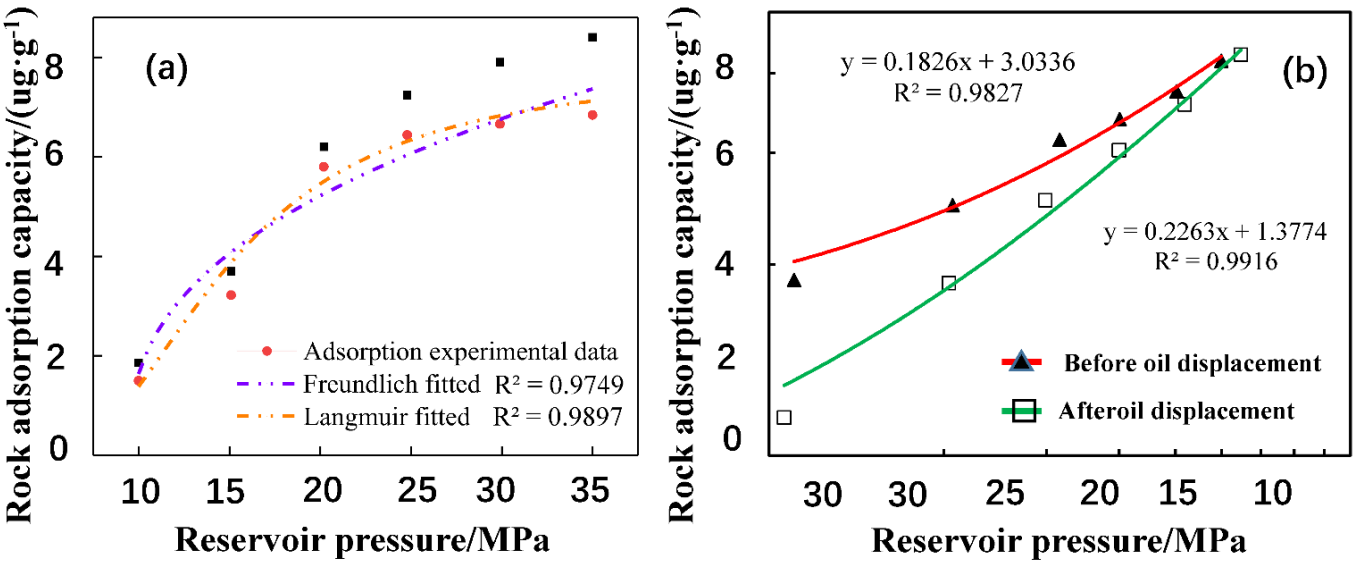

Figure 2. Data fitting of a physical model for the adsorption/desorption of methane molecules on the surface of a geological reservoir.

between reservoir pressure and methane adsorption capacity is observed, with a particularly pronounced increase at lower pressure ranges. However, at elevated reservoir pressures, methane adsorption on the reservoir surface no longer increases significantly, indicating the attainment of an adsorption equilibrium state [26].

Furthermore, Figure 2(b) demonstrates that methane molecules adsorbed on the reservoir rock undergo rapid desorption upon pressure reduction, and the desorbed amount exhibits an approximately linear relationship with reservoir pressure. This proportional relationship is consistent with the Freundlich adsorption model, indicating that the experimental configuration and quantitative analysis methods employed in this study are suitable for investigating the adsorption–desorption behaviour of methane hydrates on geological reservoir surfaces.

3.2 Influence of CO_2 fracturing fluid composition on desorption behavior

As a key driving agent acting on methane adsorbed on reservoir surfaces within fractures, CO_2 fluid plays a critical role in methane extraction through two principal mechanisms. First, CO_2 injection promotes the displacement of methane toward deeper reservoir regions, facilitating methane accumulation and ultimately enhancing production efficiency at the production wells. Second, CO_2 competes with methane adsorbed on fracture rock surfaces, thereby inducing competitive desorption of methane. The composition of CO_2 fracturing fluid governs its competitive adsorption capability, resulting in distinct effects of CO_2 concentration on methane desorption behaviour, as illustrated in Figure 3.

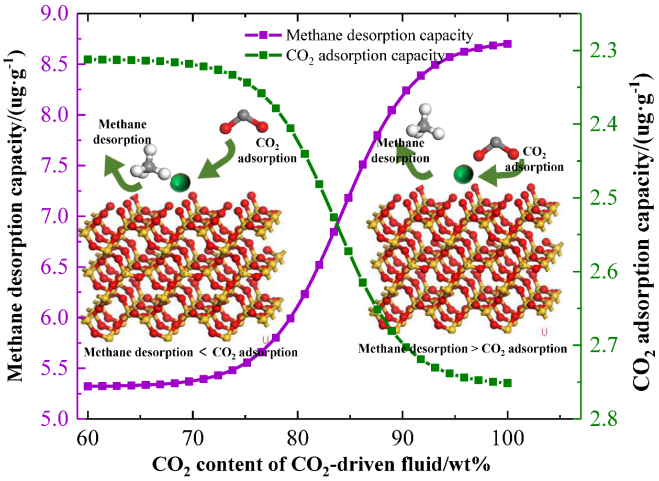

Figure 3. Conversion of methane desorption and CO_2 adsorption on the surface of reservoir rocks.

Figure 3 demonstrates a clear positive correlation between CO_2 content and the amount of methane desorbed from reservoir rock surfaces, indicating that higher CO_2 concentrations enhance the competitive desorption of adsorbed methane. Nevertheless, different CO_2 formulations exhibit distinct desorption trends, highlighting their exploratory significance for methane extraction under specific reservoir conditions. At relatively low CO_2 contents—corresponding to higher proportions of cosolvents or thickeners—the methane desorption capacity remains weak, and further increases in CO_2 content result in only marginal

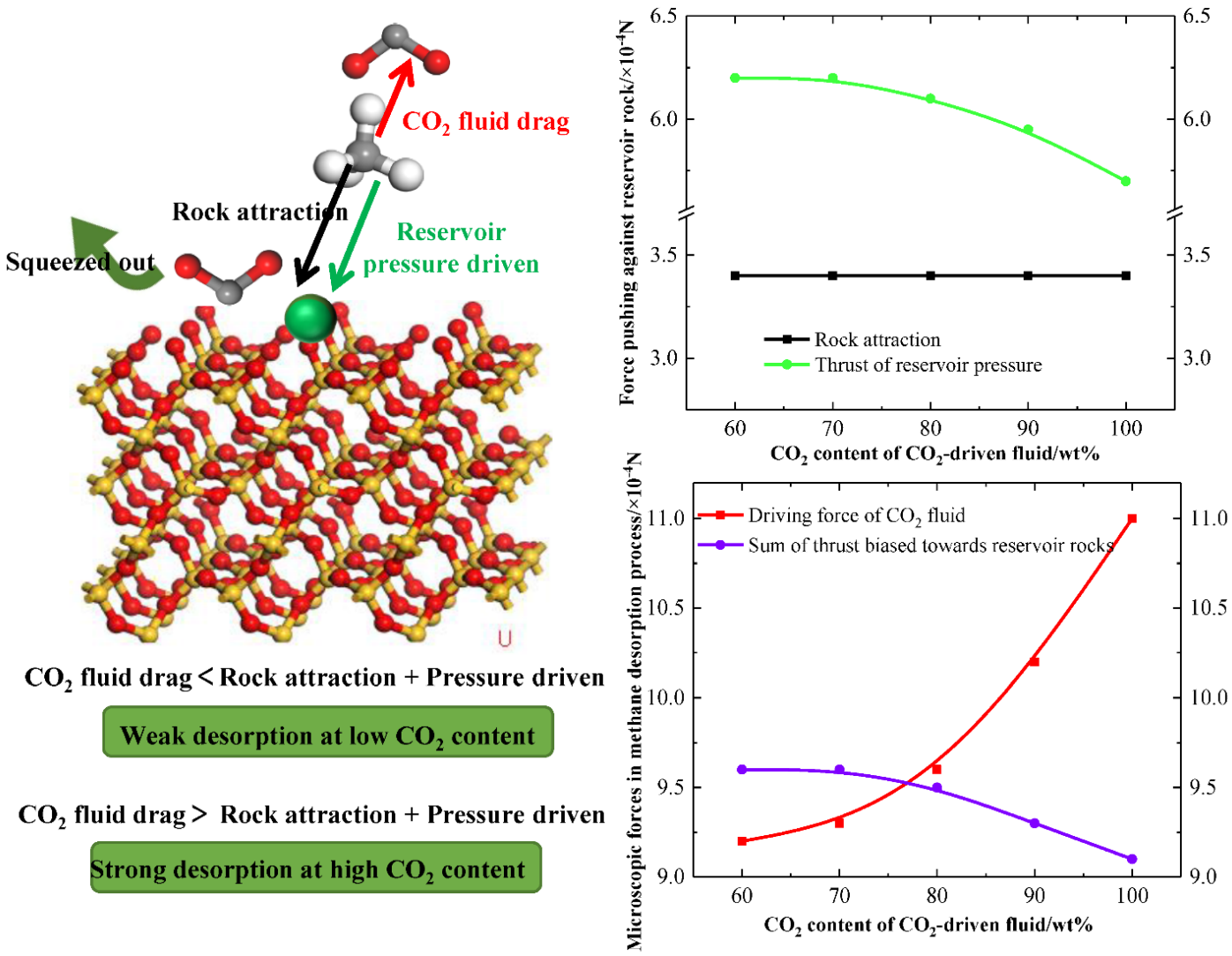

Figure 4. Force analysis of methane desorption behavior on rock surface.

improvements. In contrast, increasing the CO_2 content to 90% markedly reverses this trend, leading to a substantial enhancement in methane desorption capacity, which is critical for improving energy recovery from geological reservoirs. Specifically, a low-CO_2 formulation promotes a methane desorption capacity of only 5.3 μg/g, whereas a CO_2-rich fluid with 90% CO_2 content increases methane desorption to 8.2 μg/g within reservoir fractures.

The effect of CO_2-driven fluid composition on methane desorption behaviour at reservoir surfaces can be attributed to competitive adsorption between CO_2 and methane molecules, as well as to differences in their adsorption mechanisms. Owing to the presence of carbon atoms in both methane and CO_2 molecules, these species exhibit comparable polarity and charge characteristics, which give rise to similar interaction features with reservoir rock surfaces [27, 28]. During the initial stage of CO_2-driven fluid injection into reservoir fractures, a limited number of CO_2 molecules are adsorbed onto the rock surface, preferentially occupying available adsorption sites. As injection proceeds under pressurised conditions, methane molecules rapidly migrate toward the rock surface and occupy the remaining unfilled adsorption sites, thereby dominating the available surface sites. At this stage, the adsorption behaviour of methane and CO_2 is primarily controlled by the availability of vacant adsorption sites, and competitive adsorption between the two species remains insignificant. With increasing reservoir pressure, methane molecules continuously approach the rock surface and exhibit an enhanced tendency for adsorption. Simultaneously, methane molecules already adsorbed on rock surfaces are more strongly retained due to the increased normal force induced by injection pressure. As illustrated in Figure 4, methane adsorption during this stage is governed by three principal forces: the attractive

interaction between methane molecules and the rock surface, the pressure-driven force that pushes methane molecules toward adsorption sites, and the repulsive interaction exerted by the rock surface.

However, the displacement process is accompanied by methane desorption, which constitutes a critical mechanism for achieving efficient reservoir exploitation. During CO_2-driven displacement, CO_2 molecules form chemical associations or micro-network structures with additives such as thickeners or cosolvents, thereby generating a drag force that acts on methane molecules during fluid flow [29]. Within reservoir fractures, CO_2 molecules, while chemically associated with these additives, simultaneously interact with methane molecules adsorbed on the rock surface. Owing to the drag force induced by the micro-network structure of the driving fluid, CO_2 molecules act as an intermediate carrier that facilitates the detachment of methane molecules from adsorption sites, thereby triggering methane desorption from the reservoir surface. Methane desorption from the rock surface is predominantly governed by the drag force exerted by the CO_2-driven fluid, whereas other forces promoting methane adsorption are insufficient to counterbalance this drag effect. Moreover, increasing the CO_2 fraction in the driving fluid significantly enhances methane desorption, primarily because a higher concentration of CO_2 molecules produces a stronger collective drag force acting on adsorbed methane. A higher CO_2 content enables more CO_2 molecules to interact with individual methane molecules, resulting in greater drag and enhanced desorption. In contrast, a lower CO_2 fraction limits molecular coverage of adsorbed methane, leading to reduced drag forces and consequently diminished desorption. Therefore, as schematically depicted in Figure 4, methane desorption from reservoir rock surfaces is principally attributed to the drag force imposed by the CO_2-driven fluid, and an appropriate increase in CO_2 content is conducive to improving methane recovery efficiency in geological reservoirs.

Table 1 summarises the variations in drag force and adsorption energy exerted by the CO_2-driven fluid on methane molecules under different CO_2 compositions. These data provide quantitative insight into the methane desorption mechanisms in geological reservoirs under varying CO_2 concentrations. At low CO_2 contents, the drag force is approximately 2.5 $\times$ 10^{-3} N, whereas the adsorption energy reaches 6.2 $\times$ 10^{-4} N. With increasing CO_2 concentration to 90%, the drag force increases markedly to 4.3 $\times$ 10^{-3} N, while the adsorption energy gradually decreases to 4.8 $\times$ 10^{-4} N. The opposite trends of drag force enhancement and adsorption energy reduction with increasing CO_2 concentration corroborate the mechanistic interpretation of the desorption stage, thereby providing quantitative validation for the reliability of the proposed analysis.

Table 1. Adjustment of push-pull force and methane adsorption energy by different CO_2 components.

CO_2 contents /%	70	80	90	95	Standard deviation (n=5)
Push-pull force / $\times 10^{-3}$ N	2.5	3.1	4.3	5.1	3.5
Adsorption energy / $\times 10^{-4}$ N	6.2	5.7	4.8	4.2	5.2

3.3 Influence of reservoir temperature and pressure on desorption behavior

3.3.1 Reservoir temperature

Reservoir stimulation and energy extraction inevitably require a systematic investigation of variations in physical parameters induced by reservoir temperature and formation pressure. Methane desorption behaviour within fractures is likewise strongly influenced by these thermodynamic conditions. Figure 5 illustrates the variation in methane adsorption and desorption behaviour on rock surfaces at different temperatures, providing fundamental data for evaluating methane extraction efficiency from reservoirs at varying burial depths. As shown in Figure 5, increasing reservoir temperature significantly enhances methane desorption from fracture surfaces following hydrate dissociation, indicating a clear inverse relationship between reservoir temperature and methane adsorption capacity. At relatively low temperatures, methane molecules exhibit higher adsorption amounts on reservoir rocks, reflecting strong methane–rock interactions and correspondingly weak desorption capacity. Moreover, a gradual increase in temperature within the lower-temperature range does not induce a pronounced enhancement in methane desorption; only a modest increase is observed between 80 °C and 100 °C. In contrast, once the reservoir temperature exceeds 100 °C, the methane desorption rate rises sharply, with the desorption amount increasing rapidly to 9.4 μg/g at 120 °C. Although the experimental temperatures exceed those typical of hydrate reservoir conditions (< 20 °C), such elevated temperatures were intentionally employed to accelerate desorption kinetics and facilitate the determination of thermodynamic

parameters. The pronounced desorption behavior observed at temperatures above 100 °C provides a valuable theoretical reference for the development and optimization of thermal stimulation recovery strategies.

The physical adsorption of methane on reservoir rock surfaces following hydrate decomposition is generally regarded as a typical exothermic process, which can be effectively interpreted using the temperature-dependent expression of the Langmuir constant (Equation 3). Both the adsorption constant b and the adsorption enthalpy ΔH_{ads} of methane on the reservoir rock surface exhibit an inverse relationship with reservoir temperature [30, 31]. Consequently, increasing reservoir temperature leads to a reduction in both the adsorption constant and the magnitude of the adsorption enthalpy. A lower adsorption constant b reflects weaker methane–rock surface interactions, thereby facilitating methane desorption from the reservoir rock surface.

Equation 4, namely the van't Hoff equation governing adsorption enthalpy, further demonstrates an inverse dependence of the adsorption enthalpy on reservoir temperature. This relationship indicates that an increase in reservoir temperature leads to a reduction in the absolute value of the adsorption enthalpy. The progressive decrease in adsorption enthalpy consequently weakens the adsorption constant b, thereby reducing the amount of methane adsorbed onto the reservoir rock surface [32].

$$b = b_0 \exp\left(-\frac{\Delta H_{ads}}{RT}\right) \tag{3}$$

where b is the adsorption constant, and b_0 is the initial adsorption constant. ΔH_{ads} is the adsorption enthalpy. T is the reservoir temperature.

$$\frac{d \ln K}{dT} = \frac{\Delta H_{ads}}{RT^2} \tag{4}$$

where K is the adsorption equilibrium constant. R is the gas constant.

Table 2 presents the variations in representative microscopic kinetic parameters in reaction kinetics, which are crucial for elucidating the physical adsorption–desorption behavior of methane on reservoir rock surfaces. The continuously increasing entropy change (ΔS_{ads}) shown in Table 2 indicates that, with increasing reservoir temperature, the mobility of methane molecules previously adsorbed on the rock surface is enhanced, thereby promoting random Brownian motion of desorbed methane molecules. Meanwhile, the monotonic decrease in the Gibbs free energy change (ΔG) suggests that elevated reservoir temperatures favor the reverse process of methane adsorption, namely desorption, resulting in the gradual release of a substantial fraction of methane molecules originally adsorbed on the reservoir rock surface and their subsequent transport toward the production well [33].

$$k_d = A \exp\left(-\frac{E_d}{RT}\right) \tag{5}$$

where k_d is the desorption rate constant. A is the pre-exponential factor, and E_d is the desorption activation energy.

Table 2. Adjustment of dynamic parameters caused by changes in reservoir temperature.

Reservoir temperature, °C	80	90	100	110	120
$\Delta G \times 10^{-3}$ kJ/mol	-6.3	-6.5	-6.9	-7.5	-8.3
$\Delta S_{ads} \times 10^{-3}$ kJ/mol	2.1	2.2	2.4	2.7	3.1
$\Delta H_{ads} \times 10^{-3}$ kJ/mol	-4.2	-4.3	-4.5	-4.8	-5.2

The microscopic mechanism underlying the influence of reservoir temperature on methane desorption behavior can also be interpreted using the Arrhenius desorption rate equation (Equation 5), which reflects temperature-dependent changes in molecular mobility. As reservoir temperature increases, the kinetic energy of methane molecules correspondingly rises, inducing intensified random motion of methane molecules adsorbed on the rock surface. Once the molecular kinetic energy becomes sufficient to overcome the binding energy at adsorption sites, methane molecules desorb from the rock surface (Figure 6) [34]. This process provides a mechanistic explanation for enhanced methane desorption and recovery efficiency at elevated temperatures.

3.3.2 *Reservoir pressure*

Reservoir pressure plays a critical role in governing the adsorption–desorption behavior of methane on rock surfaces in geological reservoirs and therefore represents a key factor influencing methane recovery efficiency. As illustrated in Figures 2 and 6, an increase in reservoir pressure significantly enhances methane desorption from reservoir rocks, thereby facilitating methane recovery. However, the proportional relationship between pressure and

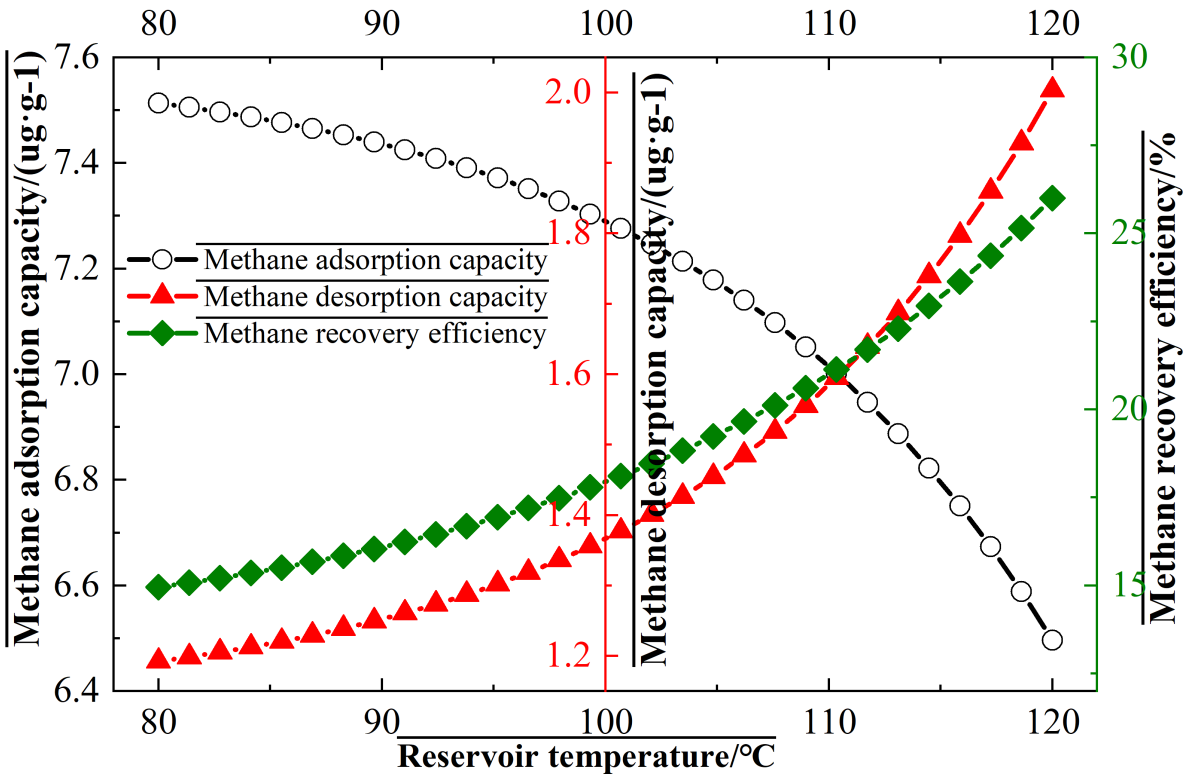

Figure 5. The variation curve of reservoir temperature on methane adsorption, desorption, and recovery rate.

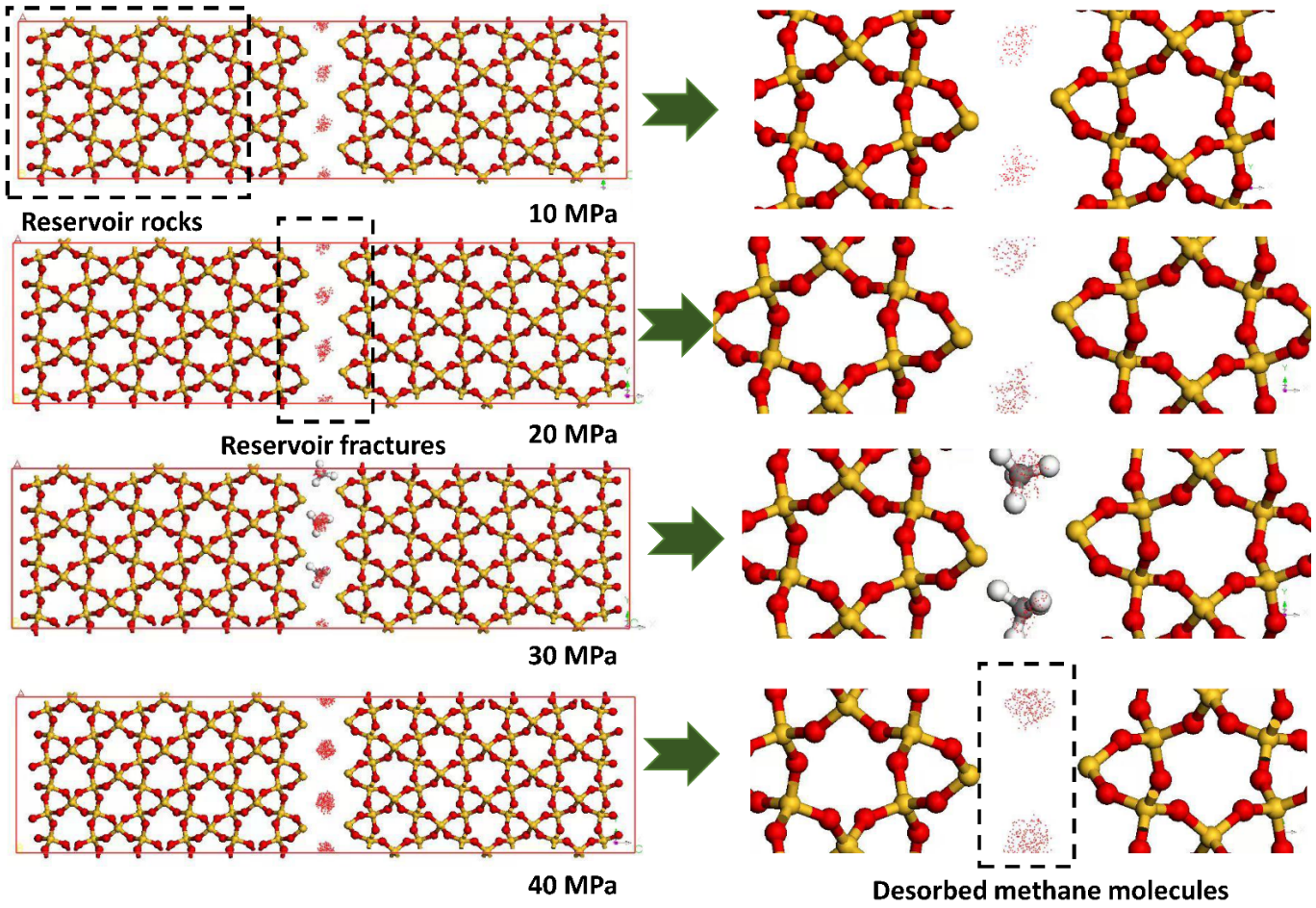

Figure 6. Changes in adsorption and desorption under different reservoir pressures.

methane desorption is not pronounced at relatively low reservoir pressures, the marginal increase in desorption indicates that low pressure is insufficient to substantially improve methane recovery efficiency. In contrast, when the reservoir pressure reaches 25 MPa, methane desorption efficiency increases sharply, which is expected to markedly enhance methane recovery during hydrate decomposition in geological reservoirs. The positive correlation between reservoir pressure and methane desorption can be attributed to variations in the net resultant forces acting on methane molecules. These forces mainly include the thrust generated by injection pressure, which drives methane molecules toward the rock surface, and the drag force exerted by CO_2 molecules flowing within reservoir fractures. Methane molecules that remain adsorbed are bound to the rock surface. Under adsorption conditions, the combined force exerted by the rock—comprising the pressure-induced thrust and rock–methane attractive interactions—exceeds the drag force imposed by CO_2 molecules. Consequently, the net force acting on methane molecules is directed toward the rock surface, hindering molecular detachment and desorption. As injection pressure continues to increase, methane molecules gradually detach from the rock surface due to a redistribution of the net force direction. Although higher injection pressure initially strengthens the thrust force toward the rock surface while leaving rock–methane attraction largely unchanged, it simultaneously intensifies the drag force exerted by CO_2 molecules on adsorbed methane (Figure 7). This drag force constitutes the dominant mechanism promoting methane desorption. Elevated injection pressure enhances intermolecular interactions within the CO_2 phase, leading to a denser microstructure and stronger molecular associations. Previous studies have demonstrated that such densification and enhanced interactions significantly increase the drag exerted by CO_2 on methane molecules. At the macroscopic scale, this enhanced drag can overcome or even surpass the combined effects of pressure-induced thrust and rock attraction, ultimately resulting in substantial methane desorption under high-pressure conditions.

Reservoir pressure not only governs the desorption behavior of methane from rock surfaces but also significantly regulates the adsorption of methane molecules onto reservoir rocks following hydrate decomposition. The adsorption process constitutes a fundamental prerequisite for elucidating subsequent methane desorption, providing an essential basis

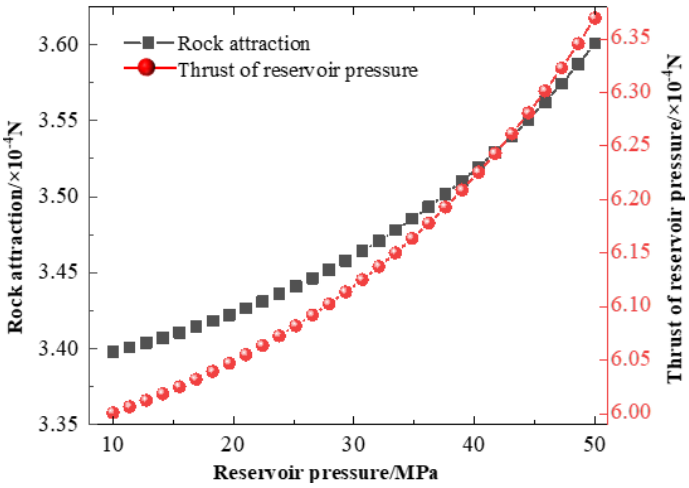

Figure 7. The influence of reservoir pressure on the thrust of methane near rocks.

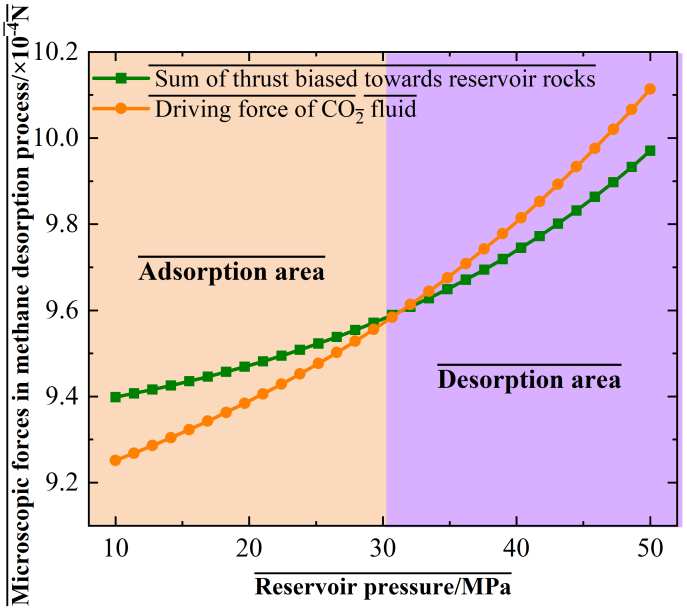

Figure 8. Comparison of changes in thrust and drag forces of methane and rock under reservoir pressure.

for understanding methane–rock interactions and revealing the underlying desorption mechanisms. As illustrated in Figures 7 and 8, the three dominant forces acting on methane molecules at the rock surface vary markedly with reservoir pressure, thereby substantially modifying the attachment state of methane. Under relatively low reservoir pressures, methane molecules in proximity to the rock surface are subjected to both injection-pressure-induced thrust and attractive forces exerted by rock adsorption sites, resulting in a net force that favors methane adsorption. Although methane molecules are simultaneously influenced by the drag force exerted by CO_2 molecules within fractures [35, 36], this drag remains insufficient to overcome the combined

thrust and attractive forces driving methane toward the rock surface. Consequently, under low-pressure conditions, methane predominantly exists in an adsorbed state. With increasing reservoir pressure, the drag force exerted by CO_2 molecules is markedly enhanced and can exceed the opposing forces responsible for methane adsorption on rock surfaces, despite the concurrent increase in adsorption-related forces [37]. The intensified drag force acting on methane molecules adsorbed on the rock surface, particularly within increasingly open fracture networks, induces pronounced methane desorption. This pressure-enhanced desorption behavior ultimately contributes to improved methane recovery efficiency from geological reservoirs [38, 39].

3.4 Influence of rock composition on methane desorption in rocks

The lithological composition of geological reservoirs is a critical factor governing the adsorption–desorption behavior of methane on rock surfaces following hydrate decomposition. Different mineralogical constituents exhibit varying degrees of affinity or repulsion toward methane molecules, thereby exerting a pronounced influence on methane recovery efficiency. As illustrated in Figure 9, distinct rock types show substantial differences in methane adsorption and desorption behaviors, with notable variations in both adsorption capacity and desorption rate. In particular, the methane desorption capacities of kaolinite, illite, and montmorillonite differ markedly, directly controlling methane recovery performance in geological reservoirs. Figure 9 indicates that methane desorption is most pronounced on illite, implying a relatively weak methane adsorption capacity. This enhanced desorption behavior is primarily attributed to the exceptionally low adsorption enthalpy of methane on illite (-12 -20 kJ/mol), which reflects a relatively weak adsorption energy [40, 41]. Under such conditions, externally injected driving fluids can more readily overcome the adsorption forces and mobilize methane molecules from adsorption sites on the illite surface, thereby reducing methane retention and enhancing recovery efficiency in illite-dominated reservoirs. The low adsorption enthalpy of methane on illite is closely related to its mineralogical structure. The abundance of surface oxygen atoms reduces the van der Waals attraction between illite and methane molecules, while the strong electrostatic interactions associated with exchangeable interlayer cations (primarily K^+) constrain structural flexibility and further weaken methane–surface interactions. Together, these factors fundamentally account for the low adsorption enthalpy and the pronounced desorption tendency of methane on illite. Moreover, the relatively small interlayer spacing of illite (1 nm) limits its capacity to stably accommodate large quantities of methane, which inevitably promotes the rapid desorption of weakly adsorbed methane molecules from the illite surface.

The methane desorption capacity on kaolinite is significantly weaker than that on illite, whereas its adsorption capacity is markedly higher. This contrast arises primarily from the intrinsic layered structure of kaolinite, which governs the magnitude and direction of the forces controlling methane adsorption and desorption, thereby leading to distinct interfacial interaction behaviors compared with illite. In kaolinite, silicon–oxygen tetrahedra are located within the inner layers of the crystal structure, while aluminum–oxygen octahedra are exposed on the outer surface. This specific structural configuration critically determines the adsorption enthalpy of methane and the balance among the three dominant forces acting on methane molecules at the mineral surface (Figure 10), thereby influencing their adsorption–desorption behavior. The relatively high adsorption enthalpy of methane on kaolinite can be attributed to the resultant force direction arising from the competition between the force driving methane molecules toward the rock surface and the force pulling them away from it [42]. To elucidate this mechanism, a comparative analysis of the three acting forces on kaolinite and illite surfaces is required. Under constant reservoir pressure, the pressure-enhancement effect associated with injection pressure is absent, and a fixed composition of the CO_2-driven fluid implies that the drag force exerted by CO_2 molecules on methane within fractures remains essentially unchanged. Consequently, the disparity in methane desorption behavior between kaolinite and illite surfaces is predominantly controlled by the intrinsic attractive interaction between the mineral surface and methane molecules, which represents the key factor governing adsorption–desorption characteristics. The polar functional groups exposed on the outermost surface of kaolinite induce electrostatic repulsion with methane molecules, thereby weakening the net attractive force between methane and the mineral surface. The progressive reduction in the thrust directing methane toward the rock surface leads to a decrease in adsorption enthalpy, which ultimately facilitates enhanced methane desorption from the

kaolinite surface.

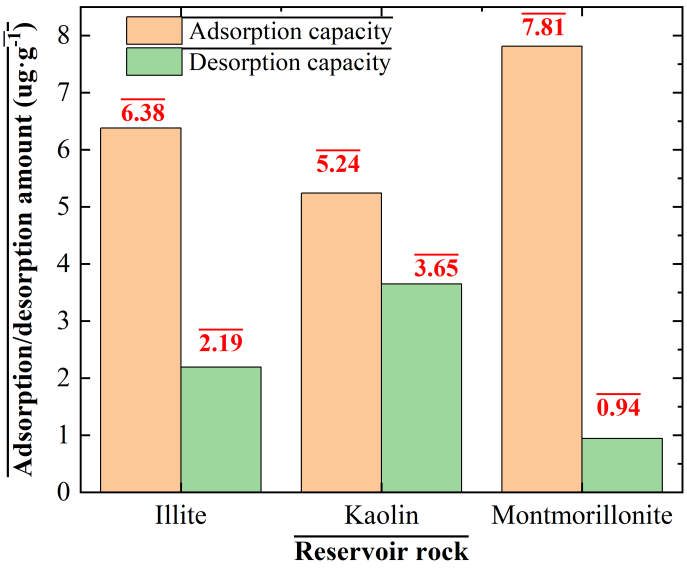

Figure 9. The distribution of methane adsorption and desorption varies among different reservoir rocks.

Montmorillonite exhibits methane adsorption–desorption behavior in reservoir fractures that is distinctly different from that of other clay minerals, providing valuable practical insights for the development of geological reservoirs with unique lithological compositions. As illustrated in Figure 9, montmorillonite shows the weakest methane adsorption capacity, corresponding to the lowest adsorption enthalpy among the examined mineral types [43]. Concurrently, the methane desorption is least pronounced on illite and kaolinite, indicating a pronounced advantage for efficient methane recovery in reservoirs enriched with montmorillonite. The minimal adsorption and maximal desorption capacity of methane on montmorillonite can be primarily attributed to its unique layered crystal structure, which fundamentally alters the force balance acting on methane molecules adsorbed at the rock surface. In the structural layers of montmorillonite, polar functional groups are located within the interlayer region, facilitating the ingress of formation water molecules and promoting extensive lattice substitution. This substitution results in the formation of a diffuse electric double layer composed of exchangeable cations, which generates a strong electrostatic repulsive force as methane molecules approach or adsorb onto the montmorillonite surface. Such repulsion substantially weakens, or even counteracts, the intrinsic attraction between the rock matrix and methane molecules, while the drag force exerted by CO_2 fluid and the thrust associated with injection pressure remain largely unchanged. Moreover, the large interlayer spacing of montmorillonite (>1.47 nm) provides a favorable structural environment for water penetration and cation exchange, further diminishing the rock–methane attractive interaction. Consequently, reservoirs dominated by montmorillonite, owing to their low methane adsorption enthalpy and strong rock-induced repulsive forces, exhibit highly favorable conditions for methane desorption and enhanced recovery.

Therefore, the differences in methane adsorption and desorption behavior among various rock types can be primarily evaluated through the adsorption enthalpy of methane, which quantitatively reflects the rock's affinity for methane molecules. Among the studied minerals, montmorillonite exhibits the strongest repulsive interaction with methane, resulting in superior methane desorption and extraction efficiency. Consequently, reservoirs dominated by montmorillonite are particularly favorable for methane production, especially in medium- to fine-grained sandstone reservoirs of the Guantao Formation in the Shengli Oilfield.

3.5 Analysis of physical and microscopic parameters of methane and CO2 on reservoir rocks

3.5.1 *Molecular parameters of CO_2 and methane*

As discussed above, the adsorption–desorption behavior of methane on reservoir rock surfaces is primarily governed by the direction of the resultant force arising from three interacting forces acting on methane molecules. When the resultant force is oriented toward the reservoir rock, methane adsorption is favored, which is unfavorable for efficient methane exploitation. In contrast, when the resultant force is directed toward the fracture space, methane molecules can readily detach from the rock surface due to the dominant dragging effect exerted by external molecules, such as CO_2. The interplay among these three forces is intrinsically related to the physicochemical properties of methane and CO_2 molecules. The molecular parameters summarized in Table 3 provide important insights into the interaction mechanisms between gas molecules and reservoir rocks. The smaller kinetic diameter and linear molecular structure of CO_2 facilitate its diffusion toward rock surfaces and enable easier penetration into reservoir pores, thereby enhancing its ability to access adsorption sites and occupy surface targets [44, 45]. In contrast, the larger kinetic

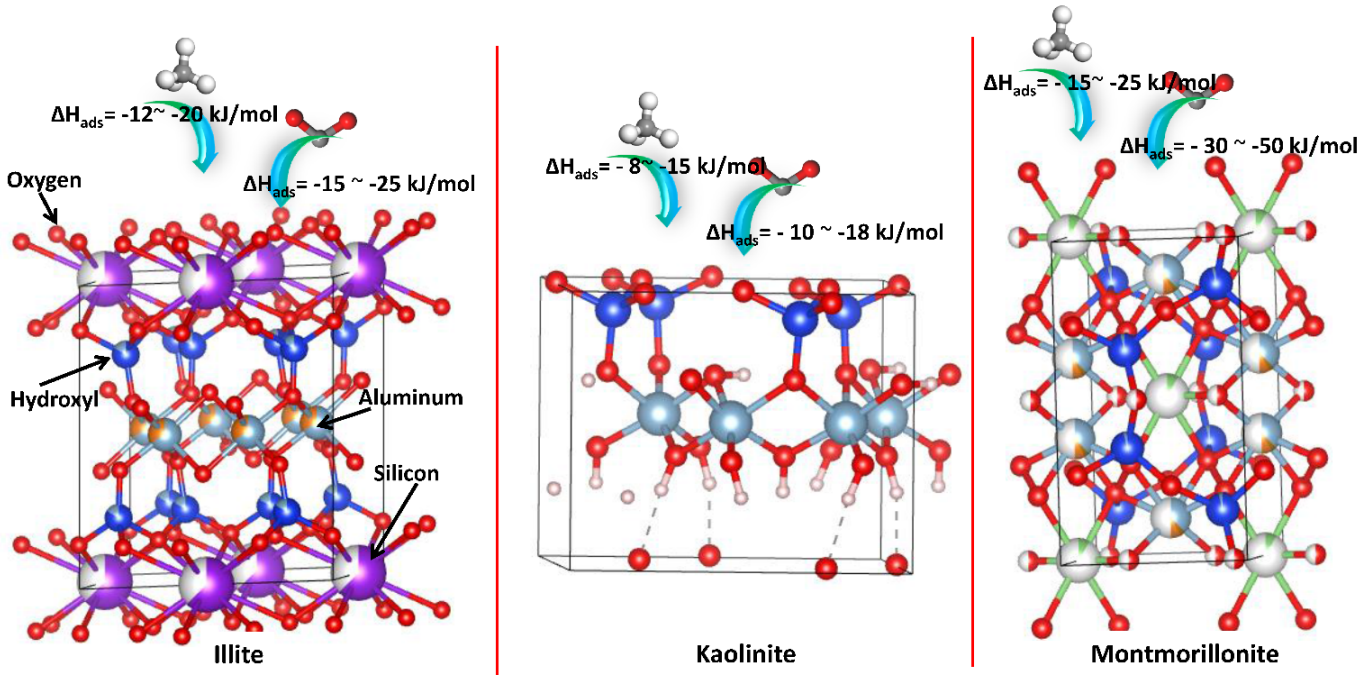

Figure 10. Adsorption enthalpy of CO2 and methane on three types of rocks [40–43].

Table 3. Physicochemical parameters of CO_2 and methane molecules.

Molecular type	Spatial Form	solid diameter/nm	vaporization temperature/K	Quadrupole moment / 10^{-26} esu cm^2
CO_2	Linear triatomic	0.33	194	-7.5
Methane	Tetrahedral	0.38	111	-4.8

diameter and quasi-spherical molecular geometry of methane limit its competitive ability for adsorption sites on rock surfaces. Moreover, the lower boiling point of methane allows it to vaporize more readily than CO_2 under identical thermal conditions, which promotes methane desorption and spillover in geological reservoirs. In addition, CO_2 possesses a significant quadrupole moment, which strengthens its electrostatic interactions with reservoir rocks and enhances its adsorption affinity. By comparison, methane is electrically neutral (quadrupole moment = 0), which is unfavorable for strong interactions with rock surface sites and fundamentally accounts for its lower adsorption enthalpy [46]. Finally, the comparable polarizability of methane and CO_2 exerts a negligible influence on their competitive adsorption behavior, indicating that this parameter does not play a dominant role in the adsorption/desorption processes and therefore requires no further consideration.

3.5.2 *Material replacement coefficient and adsorption affinity on reservoir rocks*

The separation coefficient between methane and CO_2 on reservoir rock surfaces plays a critical role in governing their competitive adsorption and desorption behaviors. As summarized in Table 4, the separation coefficients of methane and CO_2 on identical rock substrates provide an additional quantitative perspective for elucidating the mechanistic insights derived from the constructed molecular dynamics model. A separation coefficient (α) greater than unity indicates that CO_2 preferentially occupies adsorption sites on the rock surface, thereby displacing adsorbed methane molecules and promoting enhanced methane desorption [47]. Moreover, the results presented in Table 4 demonstrate that the recovery efficiency of methane displaced by CO_2 in shale reservoirs is significantly higher than that in reservoirs enriched with kaolinite, which can be attributed to the relatively higher montmorillonite content commonly present in shale formations. In addition, Table 4 reveals that an increase in reservoir temperature leads to a gradual rise in the separation coefficient α, further confirming that elevated reservoir temperatures facilitate methane desorption, consistent with the trends observed in Figure 5.

The adsorption affinity of gas molecules on reservoir rock surfaces is a critical parameter governing adsorption behavior and plays a decisive role

Table 4. The separation coefficient of methane and CO_2 molecules on reservoir rocks [48].

Rock type	Reservoir pressure/MPa	T/K	α_{CO_2/CH_4}
Wufeng Shale	0–1.80	318	4.33
Longmaxi Shale	0–1.80	318	7.04
Kaolinite	0–1.80	328	1.61

in competitive CH_4/CO_2 adsorption and methane recovery processes. Table 5 summarizes the adsorption affinities of methane and CO_2 on different reservoir rock surfaces. The results indicate that the adsorption affinity of CO_2 consistently exceeds that of CH_4 across all examined rock types, which is consistent with the preferential adsorption of CO_2 reflected by the separation coefficient (α) values in Table 4. Specifically, the difference in adsorption affinity between CO_2 and CH_4 is considerably larger in montmorillonite-rich shale (Weiyuan shale: $\Delta K = 0.25$; Youyang shale: $\Delta K = 0.54$) than in kaolinite ($\Delta K = 0.04$), indicating that montmorillonite-bearing formations exhibit a markedly stronger competitive advantage for CO_2 over CH_4 adsorption. This observation is consistent with the simulation results showing that the adsorption enthalpy of CO_2 on reservoir rocks is higher than that of methane, and provides quantitative support for the superior methane desorption performance in montmorillonite-dominated reservoirs observed in Figure 9.

Table 5. The adsorption affinity of methane and CO_2 molecules on reservoir rocks [49].

Rock type	CO_2		CH_4	
	T/K	K_{CO_2}	T/K	K_{CH_4}
Weiyuan shale	318	0.32	318	0.07
Youyang shale	318	0.65	318	0.11
Kaolinite	328	0.16	328	0.12

3.6 Impact of Residual Water

In natural geological reservoirs, methane hydrate dissociation inevitably introduces liquid water into the pore space. Previous studies [46] have demonstrated that water molecules exhibit stronger competitive adsorption on clay mineral surfaces due to their high polarity. This implies that the presence of residual water may facilitate the desorption of adsorbed methane through adsorption-site displacement. However, at higher water saturations, the formation of continuous water films can obstruct narrow pore throats, thereby increasing mass transfer resistance during methane desorption. Future work will incorporate varying levels of water saturation to further enhance the predictive capability and robustness of the proposed evaluation framework.

4 Conclusion

This study systematically investigated the methane adsorption–desorption behavior in reservoir rocks and developed a novel experimental apparatus capable of effectively simulating methane desorption following hydrate decomposition. The results demonstrate that reservoir temperature exerts a significant positive influence on methane desorption, markedly promoting methane release and enhancing recovery potential. In contrast, reservoir pressure shows a promoting effect at elevated pressures (above 25 MPa), substantially enhancing desorption efficiency and acting as a key limiting factor in methane extraction. Furthermore, the composition of the driving fluid plays a crucial role in regulating methane desorption behavior, suggesting that appropriate fluid design can substantially improve methane recovery performance. Overall, these findings provide important insights into the controlling mechanisms of methane desorption and offer theoretical guidance for optimizing gas production strategies in hydrate-bearing reservoirs.

Data Availability Statement

Data will be made available on request.

Funding

This work was supported without any funding.

Conflicts of Interest

Longhao Tang, Tingyi Wang, Yunlei Liu and Haigang Zhou are affiliated with the Shengli Oilfield Technology Inspection Center, Sinopec, Dongying 257000, China. The authors declare that this affiliation had no influence on the study design, data collection, analysis, interpretation, or the decision to publish, and that no other competing interests exist.

AI Use Statement

The authors declare that no generative AI was used in the preparation of this manuscript.

Ethical Approval and Consent to Participate

Not applicable.

References

[1] Song, Y., Yang, L., Zhao, J., Liu, W., Yang, M., Li, Y., ... & Li, Q. (2014). The status of natural gas hydrate research in China: A review. *Renewable and Sustainable Energy Reviews, 31*, 778-791. [CrossRef]

[2] Koh, C. A. (2002). Towards a fundamental understanding of natural gas hydrates. *Chemical Society Reviews, 31*(3), 157-167. [CrossRef]

[3] Makogon, Y. F. (2010). Natural gas hydrates–A promising source of energy. *Journal of natural gas science and engineering, 2*(1), 49-59. [CrossRef]

[4] Li, X. S., Xu, C. G., Zhang, Y., Ruan, X. K., Li, G., & Wang, Y. (2016). Investigation into gas production from natural gas hydrate: A review. *Applied energy, 172*, 286-322. [CrossRef]

[5] Yu, Y. S., Zhang, X., Liu, J. W., Lee, Y., & Li, X. S. (2021). Natural gas hydrate resources and hydrate technologies: a review and analysis of the associated energy and global warming challenges. *Energy & Environmental Science, 14*(11), 5611-5668. [CrossRef]

[6] Yang, M., Zhao, J., Zheng, J. N., & Song, Y. (2019). Hydrate reformation characteristics in natural gas hydrate dissociation process: A review. *Applied Energy, 256*, 113878. [CrossRef]

[7] Pang, X. Q., Chen, Z. H., Jia, C. Z., Wang, E. Z., Shi, H. S., Wu, Z. Y., ... & Wang, T. (2021). Evaluation and re-understanding of the global natural gas hydrate resources. *Petroleum Science, 18*(2), 323-338. [CrossRef]

[8] Ye, J. L., Qin, X. W., Xie, W. W., Lu, H. L., Ma, B. J., Qiu, H. J., ... & Bian, H. (2020). The second natural gas hydrate production test in the South China Sea. *China Geology, 3*(2), 197-209. [CrossRef]

[9] Qin, X. W., Lu, J. A., Lu, H. L., Qiu, H. J., Liang, J. Q., Kang, D. J., ... & Kuang, Z. G. (2020). Coexistence of natural gas hydrate, free gas and water in the gas hydrate system in the Shenhu Area, South China Sea. *China Geology, 3*(2), 210-220. [CrossRef]

[10] Wu, N., Li, Y., Wan, Y., Sun, J., Huang, L. & Mao, P. (2021). Prospect of marine natural gas hydrate stimulation theory and technology system. *Natural Gas Industry B, 8*(2), 173-187. [CrossRef]

[11] Boswell, R., Yoneda, J., & Waite, W. F. (2019). India National Gas Hydrate Program Expedition 02 summary of scientific results: Evaluation of natural gas-hydrate-bearing pressure cores. *Marine and Petroleum Geology, 108*, 143-153. [CrossRef]

[12] Sahu, C., Kumar, R., & Sangwai, J. S. (2020). Comprehensive review on exploration and drilling techniques for natural gas hydrate reservoirs. *Energy & Fuels, 34*(10), 11813-11839. [CrossRef]

[13] Chong, Z. R., Yang, S. H. B., Babu, P., Linga, P., & Li, X. S. (2016). Review of natural gas hydrates as an energy resource: Prospects and challenges. *Applied energy, 162*, 1633-1652. [CrossRef]

[14] Wei, N., Pei, J., Li, H., Zhou, S., Zhao, J., Kvamme, B., ... & Xue, J. (2024). Classification of natural gas hydrate resources: Review, application and prospect. *Gas Science and Engineering, 124*, 205269. [CrossRef]

[15] Gajanan, K., Ranjith, P. G., Yang, S. Q., & Xu, T. (2024). Advances in research and developments on natural gas hydrate extraction with gas exchange. *Renewable and Sustainable Energy Reviews, 190*, 114045. [CrossRef]

[16] Liu, T., Wu, P., Chen, Z., & Li, Y. (2022). Review on carbon dioxide replacement of natural gas hydrate: research progress and perspectives. *Energy & Fuels, 36*(14), 7321-7336. [CrossRef]

[17] Yan, C., Ren, X., Cheng, Y., Song, B., Li, Y., & Tian, W. (2020). Geomechanical issues in the exploitation of natural gas hydrate. *Gondwana Research, 81*, 403-422. [CrossRef]

[18] Yamamoto, K., Boswell, R., Collett, T. S., Dallimore, S. R., & Lu, H. (2022). Review of past gas production attempts from subsurface gas hydrate deposits and necessity of long-term production testing. *Energy & Fuels, 36*(10), 5047-5062. [CrossRef]

[19] Zhao, D., Li, X., Feng, Z., Pu, Y., Chang, H., & Jia, Y. (2022). Study on the behavior and mechanism of methane desorption-diffusion for multi-scale coal samples under multi-temperature conditions. *Fuel, 328*, 125332. [CrossRef]

[20] Xu, H., Qin, Y., Yang, D., Wang, G., Huang, Q., & Zhang, F. (2024). Experimental investigation of gas diffusion kinetics and pore-structure characteristics during coalbed methane desorption within a coal seam. *Gas Science and Engineering, 121*, 205173. [CrossRef]

[21] Zou, Y., Liu, X., Nie, B., Luo, B., Liu, P., & Zhao, X. (2023). Quantitative evaluation of the influence of injected water on methane desorption behaviors of coal in the ordos basin. Energy & Fuels, 37(22), 17227-17237. [CrossRef]

[22] Li, Y., Wang, L., Xie, Y., Wu, P., Liu, T., Huang, L., ... & Song, Y. (2023). Deformation characteristics of methane hydrate-bearing clayey and sandy sediments during depressurization dissociation. *Energy, 275*, 127527. [CrossRef]

[23] Wang, T., Deng, Z., Hu, H., Ding, R., Tian, F., Zhang, T., ... & Wang, D. (2024). Pore structure of deep coal of different ranks and its effect on coalbed methane adsorption. *International Journal of Hydrogen Energy, 59*, 144-158. [CrossRef]

[24] Ye, J., Tao, S., Zhao, S., Li, S., Chen, S., & Cui, Y. (2022). Characteristics of methane adsorption/desorption heat and energy with respect to coal rank. *Journal of Natural Gas Science and Engineering, 99*, 104445. [CrossRef]

[25] Xie, W., Wang, M., Chen, S., Vandeginste, V., Yu, Z., & Wang, H. (2022). Effects of gas components, reservoir property and pore structure of shale gas reservoir on the competitive adsorption behavior of CO2 and CH4. *Energy, 254*, 124242. [CrossRef]

[26] Li, Y., Wang, Z., Tang, S., & Elsworth, D. (2022). Re-evaluating adsorbed and free methane content in coal and its ad-and desorption processes analysis. *Chemical Engineering Journal, 428*, 131946. [CrossRef]

[27] Zhang, L., Deng, C., Guo, X., Zhang, Y., Song, L., Shi, T., ... & Li, G. (2025). Ultrasonic cavitation response mechanism of coalbed methane desorption-seepage and coal pores damage. *Process Safety and Environmental Protection, 201*, 107552. [CrossRef]

[28] Kang, J., Zhu, J., Wang, Y., Zhou, F., & Liu, Y. (2022). Dynamical modeling of coupled heat and mass transfer process of coalbed methane desorption in porous coal matrix. *International Journal of Heat and Mass Transfer, 183*, 122212. [CrossRef]

[29] Shi, P., Wang, S., Gao, Y., Yuwen, X., Ma, F., Haidong, W., & Mei, Y. (2025). Insight into the effect of fracturing thickener adsorption on coalbed methane desorption: Experiments and mechanisms. *Colloids and Surfaces A: Physicochemical and Engineering Aspects*, 137734. [CrossRef]

[30] Ren, W. (2025). Modeling hysteretic adsorption and desorption of methane on shale. *Energy & Fuels, 39*(34), 16214-16222. [CrossRef]

[31] Ming-yi, C., Zi-ting, P., Shi-bo, H., Wei-wei, S., Fu-chao, T., & Xue-jie, Z. (2025). Investigation of microstructural characteristics and methane desorption in coal using surfactant treatment. *Fuel, 401*, 135826. [CrossRef]

[32] Li, Z., Ren, T., Cheng, Y., He, X., Qiao, M., Black, D., ... & Nemcik, J. (2024). Study of methane and carbon dioxide adsorption-desorption hysteresis in coals from Sydney Basin: A theoretical and experimental approach. *International Journal of Mining Science and Technology, 34*(10), 1453-1463. [CrossRef]

[33] Huang, S., Jiang, G., Chang, Z., Wang, Q., Dong, T., He, Y., ... & Jin, Z. (2025). The effect of viscoelastic surfactant fracturing fluid on methane adsorption/desorption characteristics in Shale: Experimental and mechanistic study. *Chemical Engineering Journal, 510*, 161901. [CrossRef]

[34] Wang, Z., Deng, Z., Fu, X., Li, G., Pan, J., Hao, M., & Zhou, H. (2021). Effects of Methane Saturation and Nitrogen Pressure on N2–Enhanced Coalbed Methane Desorption Strain Characteristics of Medium-Rank Coal. *Natural Resources Research, 30*(2), 1527-1545. [CrossRef]

[35] Zhang, X., Sun, J., Liu, C., & Sun, Q. (2025). Synthesis comparative evaluation of hydrophobic polymer/surfactant fracturing fluids on methane adsorption–desorption and pore structure modifications in coal. *International Journal of Coal Science & Technology, 12*(1), 86. [CrossRef]

[36] Li, X., Si, X., Li, X., Zhang, S., Yang, T., Hu, L., ... & Li, Z. (2025). Methane release and energy evolution in coal and its implication for gas outburst. *Physics of Fluids, 37*(2). [CrossRef]

[37] Ren, J., Niu, Q., Wang, Z., Wang, W., Yuan, W., Weng, H., ... & Du, Z. (2022). CO2 adsorption/desorption, induced deformation behavior, and permeability characteristics of different rank coals: Application for CO2-enhanced coalbed methane recovery. *Energy & Fuels, 36*(11), 5709-5722. [CrossRef]

[38] Chen, X., Shi, B., Cao, Y., Long, P., Qi, Y., & Li, L. (2024). Study on the wettability and methane desorption characteristics of coal under high pressure with different surfactants. *ACS omega, 9*(18), 20012-20020. [CrossRef]

[39] Hu, X., Deng, H., Lu, C., Tian, Y., & Jin, Z. (2019). Characterization of CO2/CH4 competitive adsorption in various clay minerals in relation to shale gas recovery from molecular simulation. *Energy & Fuels, 33*(9), 8202-8214. [CrossRef]

[40] Heller, R., & Zoback, M. (2014). Adsorption of methane and carbon dioxide on gas shale and pure mineral samples. *Journal of unconventional oil and gas resources, 8*, 14-24. [CrossRef]

[41] Liang, L., Xiong, J., Liu, X., & Luo, D. (2016). An investigation into the thermodynamic characteristics of methane adsorption on different clay minerals. *Journal of Natural Gas Science and Engineering, 33*, 1046-1055. [CrossRef]

[42] Liu, D., Yuan, P., Liu, H., Li, T., Tan, D., Yuan, W., & He, H. (2013). High-pressure adsorption of methane on montmorillonite, kaolinite and illite. *Applied Clay Science, 85*, 25-30. [CrossRef]

[43] Du, X., Guang, W., Cheng, Y., Hou, Z., Liu, Z., Yin, H., ... & Shu, C. (2020). Thermodynamics analysis of the adsorption of CH4 and CO2 on montmorillonite. *Applied Clay Science, 192*, 105631. [CrossRef]

[44] Du, X., Pang, D., Zhao, Y., Hou, Z., Wang, H., & Cheng, Y. (2022). Investigation into the adsorption of CO2, N2 and CH4 on kaolinite clay. *Arabian Journal of Chemistry, 15*(3), 103665. [CrossRef]

[45] Liu, F., Ellett, K., Xiao, Y., & Rupp, J. A. (2013). Assessing the feasibility of CO2 storage in the New Albany Shale (Devonian–Mississippian) with potential enhanced gas recovery using reservoir simulation. *International Journal of Greenhouse Gas Control, 17*, 111-126. [CrossRef]

[46] Jin, Z., & Firoozabadi, A. (2014). Effect of water on methane and carbon dioxide sorption in clay minerals by Monte Carlo simulations. *Fluid Phase Equilibria, 382*, 10-20. [CrossRef]

[47] Gu, M., Xian, X., Duan, S., & Du, X. (2017). Influences of the composition and pore structure of a shale on its selective adsorption of CO2 over CH4. *Journal of Natural Gas Science and Engineering, 46*, 296-306. [CrossRef]

[48] Pei, P., Ling, K., He, J., & Liu, Z. (2015). Shale gas reservoir treatment by a CO2-based technology. *Journal of Natural Gas Science and Engineering, 26*, 1595-1606. [CrossRef]

[49] Yang, K., Zhou, J., Xian, X., Zhang, C., Tian, S., Dong, Z., ... & Cai, J. (2021). Adsorption characteristics and thermodynamic analysis of CH4 and CO2 on continental and marine shale. *Transport in Porous Media, 140*(3), 763-788. [CrossRef]

Longhao Tang received his Ph.D. from China University of Petroleum (East China) in 2022 and joined the Shengli Oilfield Technical Testing Center in the same year. Currently, Dr. Tang's research focuses on the performance evaluation of chemical agents used for reservoir stimulation and fracturing enhancement of unconventional reservoirs. (Email: 872591331@qq.com)

Tingyi Wang currently works at the Shengli Oilfield Technical Testing Center, where she mainly focuses on environmental assessment and chemical residue analysis of unconventional geological reservoirs. (Email: wangtingyi180.slyt@sinopec.com)

Yunlei Liu currently works at Sinopec Shengli Oilfield Technology Inspection Center, where his main research focuses on fracturing and acidizing of geological reservoirs and the performance evaluation of chemicals. (Email: liuyunlei.slyt@sinopec.com)

Haigang Zhou currently works at Sinopec Shengli Oilfield Technology Inspection Center, where his main research areas are geophysics and fracturing of geological reservoirs. (Email: zhouhaigang.slyt@sinopec.com)